IAI Journals.ASM.org

Hierarchies of Host Factor Dynamics at the Entry Site of *Shigella flexneri* during Host Cell Invasion

Soudeh Ehsani,[a] José Carlos Santos,[a,b] Cristina D. Rodrigues,[a] Ricardo Henriques,[c] Laurent Audry,[a] Christophe Zimmer,[c] Philippe Sansonetti,[d,e] Guy Tran Van Nhieu,[f,g] and Jost Enninga[a]

Group Dynamics of Host-Pathogen Interactions, Institut Pasteur, Paris, France[a]; Doctoral Program in Areas of Basic and Applied Biology (GABBA), Universidade do Porto, Porto, Portugal[b]; Group Imagerie et Modélisation, Institut Pasteur, Paris, France[c]; Unit Pathogénie Microbienne Moléculaire, Institut Pasteur, Paris, France[d]; INSERM Unit 789, Paris, France[e]; Interdisciplinary Research Group Intercellular Communication of Microbial Infection, College de France, Paris, France[f]; and INSERM Unit 1050, Paris, France[g]

***Shigella flexneri*, the causative agent of bacillary dysentery, induces massive cytoskeletal rearrangement, resulting in its entry into nonphagocytic epithelial cells. The bacterium-engulfing membrane ruffles are formed by polymerizing actin, a process activated through injected bacterial effectors that target host small GTPases and tyrosine kinases. Once inside the host cell, *S. flexneri* escapes from the endocytic vacuole within minutes to move intra- and intercellularly. We quantified the fluorescence signals from fluorescently tagged host factors that are recruited to the site of pathogen entry and vacuolar escape. Quantitative time lapse fluorescence imaging revealed simultaneous recruitment of polymerizing actin, small GTPases of the Rho family, and tyrosine kinases. In contrast, we found that actin surrounding the vacuole containing bacteria dispersed first from the disassembling membranes, whereas other host factors remained colocalized with the membrane remnants. Furthermore, we found that the disassembly of the membrane remnants took place rapidly, within minutes after bacterial release into the cytoplasm. Super-resolution visualization of galectin 3 through photoactivated localization microscopy characterized these remnants as small, specular, patchy structures between 30 and 300 nm in diameter. Using our experimental setup to track the time course of infection, we identified the *S. flexneri* effector IpgB1 as an accelerator of the infection pace, specifically targeting the entry step, but not vacuolar progression or escape. Together, our studies show that bacterial entry into host cells follows precise kinetics and that this time course can be targeted by the pathogen.**

Invasive pathogens such as *Shigella flexneri*, *Salmonella enterica*, or *Listeria monocytogenes* are capable of subverting host factors to induce their uptake into typically nonphagocytic epithelial and/or endothelial cells (32). This is achieved via bacterial constituents or adhesive molecules present on the pathogen surface, the secretion of soluble bacterial factors, or the translocation of effectors into the host cell through specialized molecular injection devices. Independent of the mode of interaction, the internalization process is rapid for all studied pathogens, requiring only a few minutes and featuring a complex and coordinated interplay between host and bacterial factors.

After ingestion of spoiled food or water, as few as 10 to 100 bacteria are sufficient to cause an infection resulting in mucosal ulceration and bloody diarrhea, qualifying *Shigella* as a potent enteroinvasive pathogen (20). Upon contact of *S. flexneri* with an epithelial cell, the injection of effectors through the type III secretion system (T3SS) leads to the formation of a signaling platform consisting of the bacterial translocon complex constituents IpaB and IpaC and the targeting of host factors through injected effectors (25, 37). Together, these induce a complex rearrangement of the cortical cytoskeletal components, resulting in the formation of lamelipodia that engulf the pathogen and lead to its uptake. These events are coordinated by bacterial effectors, e.g., IpgB1 and IpgB2, IpgD, or IpaC, and host factors, mainly the small GTPases of the Rho family, Rac, Cdc42, and kinases, such as Abl and Src (4, 7, 38). Apart from GTPases and kinases, other signaling molecules have been implicated in the entry process of *S. flexneri*, namely, inositol signaling, which is targeted by IpgD (7).

Examplarily, the bacterial effector IpgB1 mimics RhoG at the host plasma membrane and interferes with the ELMO/Dock180 pathway (12, 27). Furthermore, the homologous effector IpgB2, together with IpgB1, orchestrates bacterial entry through their GEF activities, which have been reported for both of them *in vitro* (11, 18). The activation of the GTPases induces members of the WASP family verprolin-homologous protein family (WAVE) that in turn activate the actin-nucleating Arp2-Arp3 complex. Additionally, it has been suggested that the C terminus of IpaC is involved in the activation of the kinase Src (24). In turn, Src and another tyrosine kinase, Abl, play a role in the bacterial entry process via the phosphorylation of CrkII at the plasma membrane, which leads to the recruitment of phosphorylated cortactin to the *S. flexneri* entry site (3, 5).

Upon internalization, *S. flexneri* is surrounded by an endocytic vacuole that is subsequently ruptured, thereby releasing the pathogen into the host cellular cytoplasm (6, 35). We have recently shown that the rupture happens within minutes after uptake and can be spotted using fluorescently labeled galectin 3 as a marker for the disassembled membranes (30, 34). It is believed that the membrane remnants are then processed into smaller ves-

Received 29 December 2011 Returned for modification 22 January 2012
Accepted 12 April 2012
Published ahead of print 23 April 2012
Editor: J. B. Bliska
Address correspondence to Jost Enninga, jostenn@pasteur.fr.
Supplemental material for this article may be found at http://iai.asm.org/.
Copyright © 2012, American Society for Microbiology. All Rights Reserved.
doi:10.1128/IAI.06391-11

icles, and it has been shown that they are targeted to the autophagy machinery by the tethering of autophagy markers to the site of ruptured membranes, which in turn leads to the induction of signaling pathways (8). Further, it has been found that autophagy-associated signaling is also triggered from *S. flexneri* surrounded by septin structures termed septin cages (22, 23).

The dynamic recruitment of host factors to the forming vacuole and to the membrane remnants upon vacuolar disruption is still poorly understood. So far, only a few studies have tracked bacterial entry into living host cells in real time compared to investigations that used endpoint assays (2, 24, 29, 34). Therefore, we aimed at obtaining a more precise picture of the temporal events surrounding the entry of *S. flexneri*. HeLa cells were transfected with a set of host factors, and the time course of their tethering to the site of bacterial entry and the disassembly of the endocytic vacuole was monitored. This allowed us to delineate the functional hierarchies of host factor recruitment during the entry process, which involves different families of signaling molecules, namely, kinases or GTPases. We observed the simultaneous recruitment of the small GTPases Rac, RhoA, and Cdc42 and of the kinases Src and Abl to the site of bacterial entry, which contrasted with a specific sequence of events for their dispersal during the process of vacuolar rupture. Further, we show that the vacuolar membranes disassemble rapidly upon release of the pathogen into the cytoplasm. Finally, we revealed that the bacterial effector IpgB1 is responsible for the rapid entry of bacteria into the host and propose that it acts as a pacemaker of infection.

MATERIALS AND METHODS

Cell culture and infection assays. All cell culture reagents were purchased from Invitrogen unless otherwise stated. Human epithelial HeLa cells were cultured in Dulbecco's modified Eagle's medium (DMEM) supplemented with 10% (vol/vol) fetal bovine serum (FBS), 50 μg/ml penicillin, 50 μg/ml streptomycin, and 2 mM L-glutamine at 37°C, 5% CO_2. All live-cell fluorescence microscopy was performed in EM buffer (120 mM NaCl, 7 mM KCl, 1.8 mM $CaCl_2$, 0.8 mM $MgCl_2$, 5 mM glucose, 25 mM HEPES, pH 7.3).

Overnight bacterial cultures were inoculated at a 1/100 dilution in tryptic casein soy broth (TCSB) with the appropriate antibiotic if required and grown to an optical density at 600 nm (OD_{600}) of ~0.3. Before infection, the bacteria were washed with PBS and coated with poly-L-lysine (Sigma Corp.) at a final concentration of 10 μg/ml to facilitate bacterial adhesion to cells. After 10 min of incubation at room temperature, the bacteria were washed 2 times with PBS, resuspended in the medium of the cells that were prepared for infection, and used immediately.

Bacterial strains. The following *S. flexneri* strains were used: *S. flexneri* M90T (wild type), *S. flexneri* M90T expressing dsRed, BS176 (no virulence plasmid), an *ipgB1* strain (nonpolar mutant of the effector IpgB1), and the complemented *ipgB1*/pHA61 strain (these strains were described previously [11, 36, 19]). All bacterial strains were grown in TCSB at 37°C. The growth medium was supplemented with kanamycin (100 μg/ml) or ampicillin (50 μg/ml), depending on the resistance of the strain used.

Plasmids and transfection. For the expression of actin-mOrange, the mOrange coding sequence was inserted into the actin-EGFP-C3 plasmid by excising the enhanced green fluorescent protein (EGFP) sequence at the NheI/XhoI sites and inserting the mOrange sequence (the primers used were as follows: 5′, AGAGCTGCTAGCATGGTGAGCAAGGGCGAGGA, and 3′, AGAGTCCTCGAGATCTGAGTCCGGACTTCTACAGCTCGTCCATGC). The construct was verified by sequencing. For the expression of galectin 3-tandem Eos fluorescent protein (tdEos), the tdEos coding sequence was inserted in the peGFP-N1 plasmid (BD Biosciences Clontech) by excising the EGFP at the BamHI/NotI sites and inserting the tdEos sequence (the primers used were as follows: 5′, AGCTGGATCCATCCACCGGTCGCCACCATG, and 3′, AGTCGCGGCCGCTCTAGAGTCGCGGCCGCTTA) and by inserting the galectin 3 coding sequence at the KpnI/BamHI sites (the primers used were as follows: 5′, ATGCGGTACCCGCCACCATGGCAGACAATTTTTCGCTC, and 3′, GCATGGATCCGTATCATGGTATATGAAGCACT). The construct was verified by sequencing. The other plasmids have been described previously, as follows: pEGFP-galectin 3 (30), pEGFP-actin (24), pOrange-galectin 3 (34), pOrange-RhoA (34), pEYFP-RhoA (17), pEYFP-Rac1 (17), pOrange-Rac1 (34), pEGFP-Abl (5), and pEGFP-Src (24).

For transfection of samples that were processed for indirect immunofluorescence, HeLa cells were plated on 12-well plates containing glass coverslips at a density of 2×10^4 cells per coverslip (diameter, 12 mm; thickness, 0.13 to 0.17 mm) 24 h before transfection. For transfection of samples that were processed for live-cell imaging, HeLa cells were seeded into glass bottom dishes 35 mm in diameter at a density of 2×10^5 cells per dish (Mattek) or 96-well glass bottom plates (Nunc) at a density of 3×10^4 cells per plate 24 h before transfection.

Microscopy and image analysis. Bacterial invasion was measured in real time on a Leica DM or Nikon inverted microscope equipped with a heated stage, using a 40× N-Plan Objective for simultaneous phase-contrast imaging (Leica or Nikon), and fluorescence imaging was performed with excitation at 465 to 500 nm (fluorescein isothiocyanate [FITC]) and 532 to 554 nm (rhodamine), and emission was detected with 516- to 556-nm (FITC) and 573- to 613-nm (rhodamine) filters. Images were captured using a Cascade 512B camera or a CoolSnap2 camera (Roeper Scientific). Images were acquired in the two fluorescent channels and in *trans* every 30 s or 90 s. Time lapse series were analyzed with the freeware program ImageJ (http://rsb.info.nih.gov/ij/) and further processed using Excel (Microsoft).

Superresolution imaging. Glass coverslips (diameter, 18 mm; thickness, 1) were cleaned using acetone (high-grade pure) treatment for 1 h, followed by overnight treatment with a potassium hydroxide solution at 0.1 M and extensive cleaning with autoclaved ultrapure water.

HeLa cells were maintained in DMEM F-12 medium (without phenol red) supplemented with 4% FBS and 1% penicillin/streptomycin. Forty-eight hours before bacterial infection, HeLa cells were seeded on the treated coverslips and transfected with 1.5 μg of the plasmid galectin 3-tdEos. For the infection assay, *S. flexneri* M90T bacterial cultures were prepared as previously described. Galectin 3-tdEos-transfected cells were incubated for 45 min with *S. flexneri* M90T at a multiplicity of infection of 100. Afterward, samples were fixed with 2% paraformaldehyde for 30 min at 37°C, washed, and incubated with 0.5 μl of fluorescent beads (2 mM 0.1-μm TetraSpeck microspheres, fluorescent blue/green/orange/dark red; Invitrogen) for 30 min. For imaging, coverslips were mounted in PBS.

Photoactivated localization microscopy (PALM) imaging was performed on a home-made setup, previously described in detail (1, 15), based on a Nikon Ti-E eclipse microscope system. For tdEos activation and imaging, the system uses a solid-state laser with an emission wavelength at 488 nm (Spectra Physics, Japan) and diode lasers with emission wavelengths at 405 nm and 561 nm (Spectra Physics, Japan). Observations were performed with a 100× oil immersion objective (numerical aperture [NA], 1.49) and detected by an electron-multiplying charge-coupled device (EM-CCD) camera (Ixon DV887ECS-BV; Andor, Belfast, Northern Ireland). Imaging was performed with a final magnification of ×150, corresponding to a pixel size of 107 nm. Sequences of 50,000 to 100,000 wide-field fluorescence images compatible with PALM were acquired with a 50-ms exposure time. During acquisition of PALM image sequences, the 561-nm laser power was kept constant for readout of the tdEos activated state, and the 405-nm laser was pulsed at decreasing frequencies adjusted manually to maintain a stable number of active fluorophores per frame. The imaging parameters were set using the μManager freeware (http://www.micro-manager.org/), and laser control was achieved with custom software (15).

After acquisition, each sequence of raw diffraction-limited images was processed with ImageJ and QuickPALM (15). The QuickPALM software

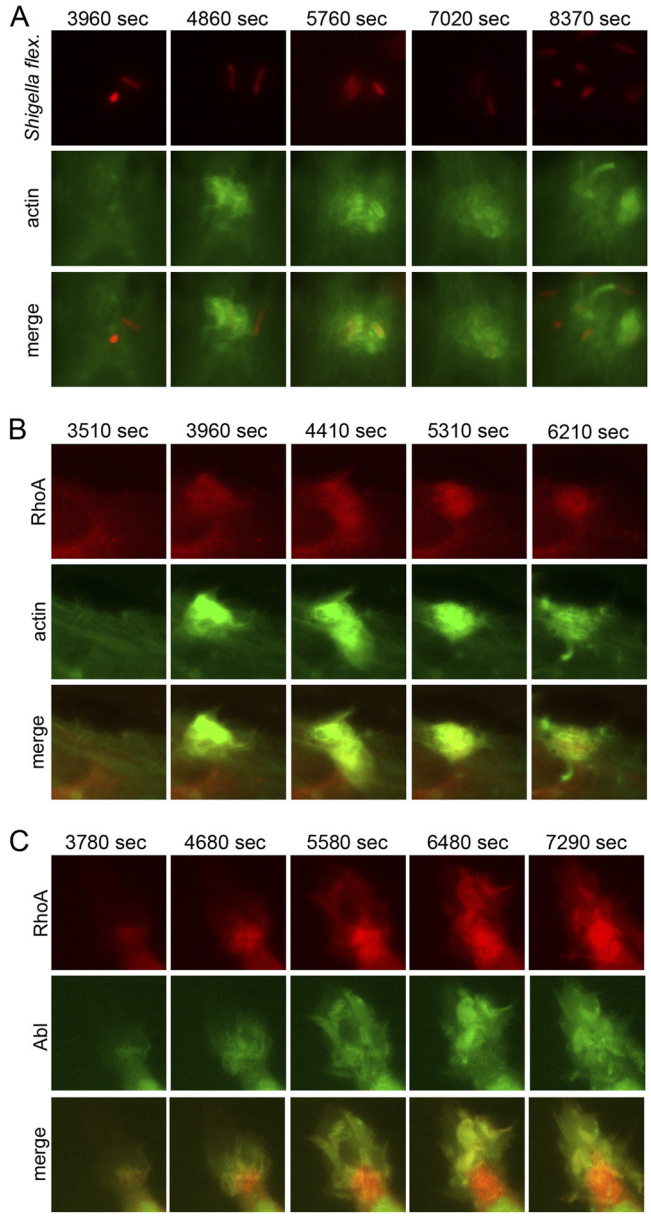

FIG 1 Sequential recruitment and dispersal of host molecules involved in the entry of *S. flexneri* into epithelial cells. (A) HeLa cells transfected with actin-EGFP were challenged with *S. flexneri* expressing dsRed and monitored by time lapse fluorescence microscopy. The recruitment of actin to the entry site highlights the successive internalization steps, bacterial contact, focus formation, collapse of the entry focus, and intracytoplasmic bacteria moving along actin tails. (B) Simultaneous tracking of host cellular actin and the small GTPase RhoA at the entry site shows that they are both recruited to the bacterial entry site at the same time. (C) Simultaneous tracking of the host cellular kinase Abl and the GTPase RhoA at the entry site shows that they are both recruited at the same time. Abl is tethered to the apical edges of the forming foci, whereas RhoA spreads diffusely through the focus and is enriched around the vacuole containing bacteria. Representative data from 5 to 10 independent experiments are shown.

computed the positions of individual molecules and reconstructed super-resolution images with an initial arbitrary pixel size of 10 nm by superimposing Gaussian spots with a full-width-Hald-maximum (FWHM) of 30 nm centered on these positions. The imaged fluorescent beads were used as fiducial markers for drift correction. To estimate the average resolution,

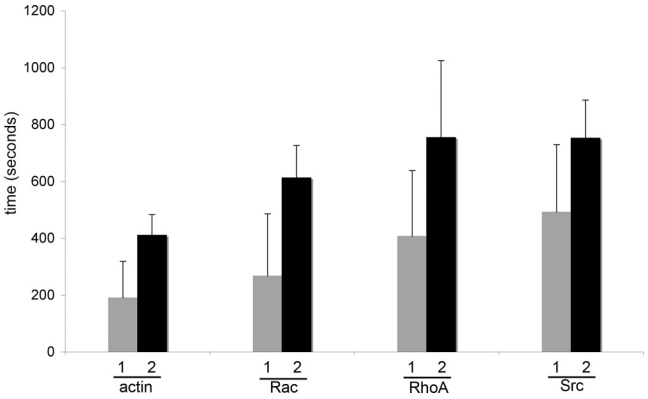

FIG 2 Quantification of the sequence of recruitment of bulk actin, small GTPases, and kinases to the entry site of *S. flexneri*. The images were quantified by thresholding from the image sequences displayed in Fig. 1 (see Materials and Methods for details). Actin, small GTPases, and kinases are rapidly recruited to the pathogen entry site (between 200 and 400 s after contact), and these factors reach their peak at the entry foci between 425 and 725 s after bacterial contact. The standard deviations (SD) (error bars) indicate high variance of the events temporally, making it impossible to delineate clear hierarchies of recruitment. 1, delay of host factor recruitment to the pathogen entry site upon bacterial contact; 2, time window between host factor recruitment and the time point with the peak of the individual foci before their disassembly. Data from 5 to 10 independent experiments are shown.

23 small clusters of galectin 3-tdEos were aligned by their center of mass, and the FWHM of the superimposed clusters was calculated, yielding an estimated resolution of 28 nm.

RESULTS

Numerous studies have described the recruitment of the host actin cytoskeleton, regulatory factors like small GTPases of the Rho family, and tyrosine kinases to the entry site of enteroinvasive bacteria, such as *Shigella* or *Salmonella* (9, 31). The studies discovered a growing family of host proteins involved in the entry process. We aimed at studying the spatiotemporal hierarchies between some representative host protein family members at the bacterial entry site throughout the successive steps of internalization during cell challenge with *S. flexneri* wild type and the *ipgB1* mutant strain.

Host proteins involved in cytoskeletal rearrangements are recruited simultaneously to the *S. flexneri* entry site. Figure 1A (for more detail, see Movie S1 in the supplemental material) displays a series of time lapse images of actin-GFP-transfected HeLa cells challenged with dsRed-expressing *S. flexneri*. These images confirm the well-documented massive actin rearrangements upon host cellular contact with the bacterium. We used such image series to establish a quantification procedure with the open-source software ImageJ to determine the time points when the accumulation of a host factor became detectable at the site of bacterial entry and when it reached its maximum at the entry site before the disassembly of the individual entry focus. These quantifications were performed in order to decipher the order of host factor recruitment at the bacterial entry site. As a control, we compared the bacterial entry kinetics in transfected cells with those of nontransfected cells and found no significant differences. We then went on to challenge HeLa cells with *S. flexneri* cotransfected with fluorescently tagged actin and members of the small GTPase family. Figure 1B (for more detail, see Movie S2 in the supplemental mate-

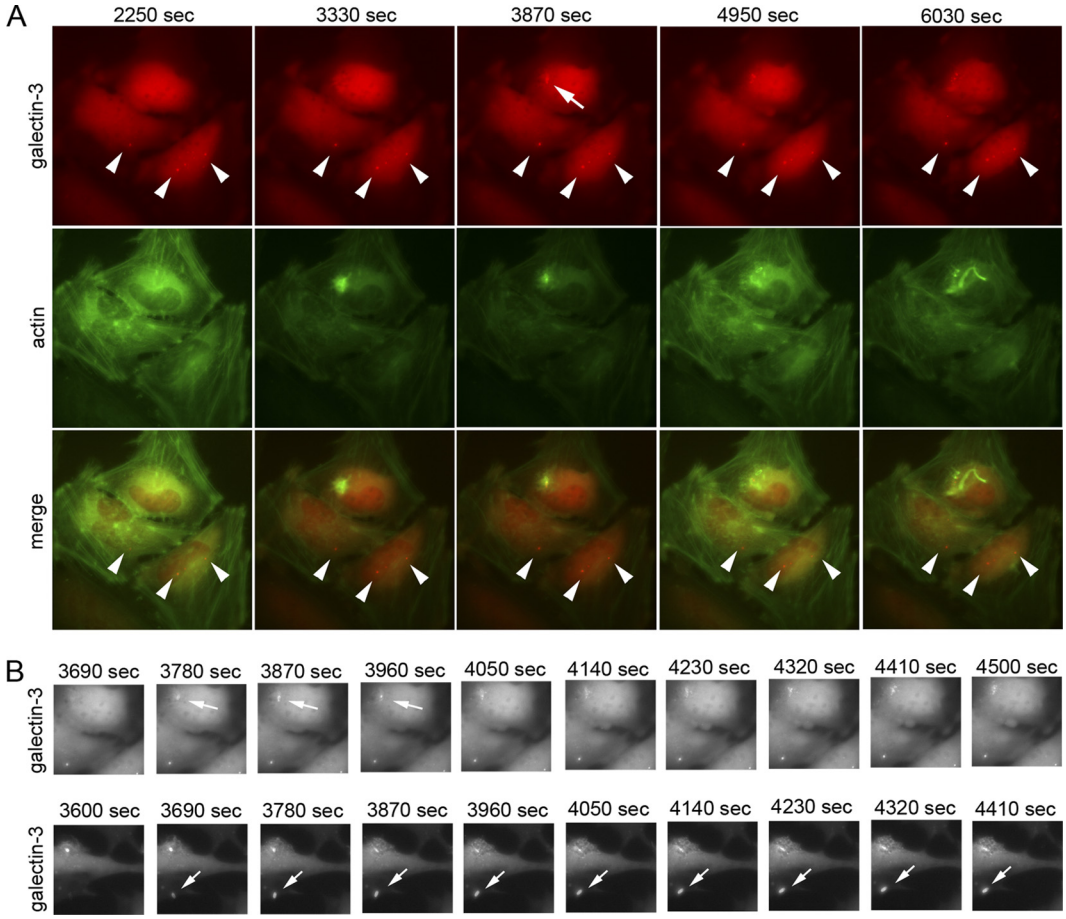

FIG 3 Rapid assembly and disassembly of galectin 3 around the ruptured membranes after vacuolar escape of *S. flexneri*. (A) Galectin 3 flags the membrane remnants upon vacuolar rupture of the pathogen. The remnants (indicated by the arrow) are typically present only for a few minutes upon membrane rupture and cannot be distinguished from background signal (arrowheads) at later time points. (B) In some instances, galectin 3 remains associated with the membrane remnants (arrows) for hours after escape from the vacuole. Representative data from at least 10 independent experiments are shown.

rial) shows that actin and RhoA are simultaneously recruited at the entry site upon challenge. Similar results were obtained with other small GTPases, such as Rac1 or Cdc42 (data not shown). Tyrosine kinase recruitment was exemplarily studied using Abl (Fig. 1C; for more detail, see Movie S3 in the supplemental material) and Src (24) (see Fig. S1 in the supplemental material) fused to EGFP. Cotransfection of Abl and RhoA showed that both were recruited to the bacterial entry site at the same time points; however, their localizations differed upon recruitment. Abl was located at the distal tips of the forming membrane ruffles, whereas the GTPases, such as RhoA, were spread throughout the entry focus or around the entering bacterium, as was previously shown for Src (24, 25). This was expected, since distinct functions during the entry process have previously been attributed to the different recruited host factors (25, 28).

Next, we quantified the fluorescence intensities at the *S. flexneri* entry sites, setting stringent thresholds in the ImageJ software. The time point of the start of host factor recruitment was determined as the time point when fluorescence values were at least 50% above the background levels before bacterial contact. Then, we determined the time span between this time point and the time point of bacterial contact that could be identified in the TRANS channel (1 in Fig. 2). Second, we measured the mean fluorescence intensity in the area of bacterial entry and determined the time point when it reached its maximum. We then subtracted the time point of bacterial contact from the time point when a maximum mean fluorescence intensity was present within the entry focus. This was used to determine the time it took to reach maximal host factor recruitment, coordinating the cytoskeletal rearrangements at the entry site (2 in Fig. 2). Figure 2 depicts the summary of these quantifications for the recruitment of actin, Rac1, RhoA, and Src. Strikingly, we found that all these factors are recruited simultaneously at the bacterial entry site upon bacterial contact, and the large standard deviations show pronounced variability at the single-cell level (Fig. 2, columns numbered 1). Further, recruitment of the analyzed host factors appeared rapidly upon contact, within 200 to 400 s. Similar results were obtained when analyzing the time it took to reach maximal recruitment of host factors to the entry foci. Here, we found again that the maxima were reached within similar time intervals for all measured host factors and that the standard deviations were pronounced for all analyzed scenarios, highlighting large variability in the kinetics of the entry process. We also realized that there is some variability in the diminishing of the recruited host factor signals at the entry site, e.g., the massive early actin recruitment disappeared before the RhoA sig-

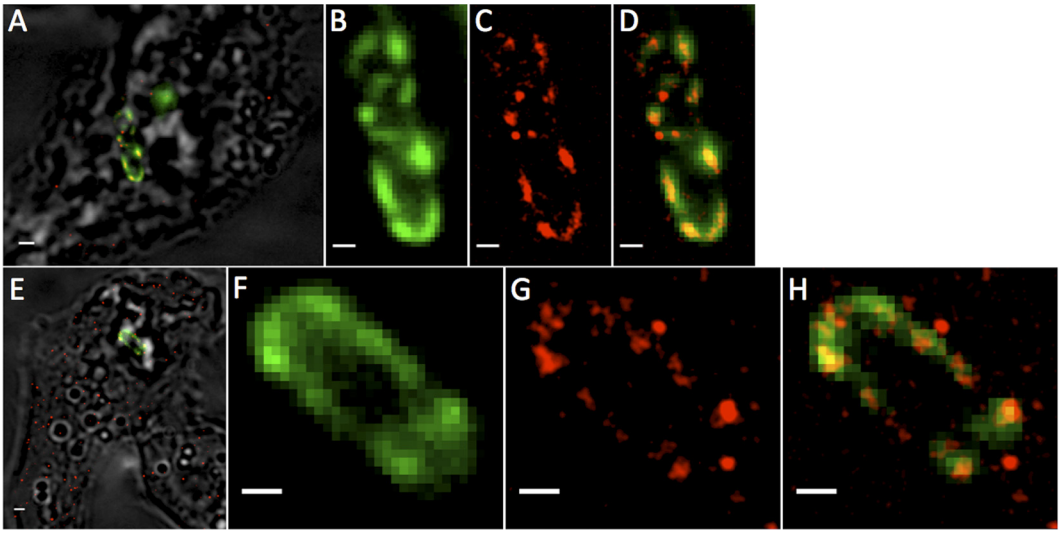

FIG 4 High-resolution analysis of disassembling vacuoles by superresolution microscopy. (A to H) HeLa cells transfected with galectin 3-tdEos fluorescent protein (tdEosFP) were infected with *S. flexneri* M90T. PALM shows galectin 3-tdEos being organized in heterogeneous patchy clusters in the bacterial enveloping vacuoles. The images correspond to two different acquisitions representative of a total of 7 cells from 2 independent experiments. (A and E) Merges of the bright-field (gray), wide-field epifluorescence (green), and superresolution PALM (red) images. (B to D and F to H) Zoomed images of the bacterial region. (B and F) Wide-field epifluorescence. (C and G) PALM imaging. (D and H) Merges of wide-field epifluorescence and PALM imaging. Scale bars: A and E, 1,000 nm; B to D and F to H, 500 nm.

nal in Fig. 1B. However, we have not been able to establish a reliable algorithm to quantify this phenomenon.

Disassembly of the ruptured vacuolar membrane remnants is highly dynamic. We went on to investigate the subsequent step of *S. flexneri* invasion, bacterial escape from the endocytic vacuole. In particular, we were interested in tracking the fate of the disassembling membranes that constituted the endocytic vacuole containing bacteria using the recently described marker galectin 3 (30). It has been shown that fluorescently tagged galectin 3 is recruited to the bacterial entry site within seconds after vacuolar rupture and that it targets the disassembling membranes surrounding the bacterium (30, 34). By cotransfecting HeLa cells with actin-EGFP and galectin 3-mOrange, we confirmed this rapid recruitment of galectin 3 to the entering bacteria, which highlights the ruptured membranes as "bacterial ghost-like" structures (Fig. 3A and B, top; see Movie S1 in the supplemental material for more details). Strikingly, our time lapse experiments demonstrated that the galectin 3 vacuolar-membrane-wrapping signal was very short-lived, disappearing within 5 to 15 min after bacterial escape from the vacuole (Fig. 3A, arrow). At later time points, the galectin 3 signal was similar to background signals in cells that were not invaded by *S. flexneri* (compare the specific signal, indicated by an arrow, and the nonspecific background signals, indicated by arrowheads, in Fig. 3A). In a few cases, galectin 3 highlighted the bacterial ghost-like structures for more than 30 min without disassembling into smaller membrane vesicles. However, it turned out to be difficult to quantify the extent of this phenomenon, due to the heterogeneity of the measured signal (Fig. 3B, arrows in the bottom row). Together, these findings show the rapid processing of the disassembling membranes at the bacterial entry site that are subsequently targeted to autophagy (8).

To analyze the membrane disassembly in more detail, we performed PALM, which achieves a 10-fold increase in resolution over the classical optical limit in microscopy (roughly 30 nm versus 300 nm) (1, 16). PALM imaging of the photoactivatable tdEos fused to galectin 3 was used to obtain superresolution insight into the cellular localization of the protein upon the rupture of the vacuole containing bacteria.

HeLa cells were transfected with galectin 3-tdEos and infected with *S. flexneri* M90T. We selected seven different individual fixed cells featuring visible galectin 3 staining accumulating around the ruptured membranes of the invading bacteria and superresolved them through PALM imaging. Two representative samples are shown in Fig. 4A to D (first example) and E to H (second example). PALM allowed us to discern small patchy accumulations of galectin 3 in the vicinity of the bacteria (Fig. 4C and G). Importantly, no structures with a lumen (resembling vesicles) could be observed. Further analyses of the cluster sizes of these small accumulations of galectin 3 permitted us to observe a distribution of sizes ranging from 30 nm (the estimated resolution of PALM images) to 300 nm in diameter (see Fig. S2 in the supplemental material). These structures are beyond the resolution limit of standard wide-field epifluorescence microscopy and thus cannot be accurately discerned by standard imaging methods (Fig. 4B and F). Larger clusters of galectin 3 with diameters between 100 and 200 nm are found predominantly in the vicinity of the disassembling bacterial vacuole, but not in the rest of the host cellular cytoplasm (see Fig. S2 in the supplemental material), indicating the vacuolar degradation surrounding the bacteria.

We then investigated the localization of the simultaneously recruited host factors (Fig. 1 and 2) at the site of the vacuole containing bacteria around the time of vacuolar escape. In contrast to their recruitment to the entry site, we found that the disassembly process showed a higher level of organization with regard to the temporal sequence of events. We found that the accumulated actin surrounding the bacteria within vacuoles diminished before the recruitment of galectin 3 (Fig. 5A and C; for more detail, see Movie S5 in the supplemental material). Interestingly, the galectin

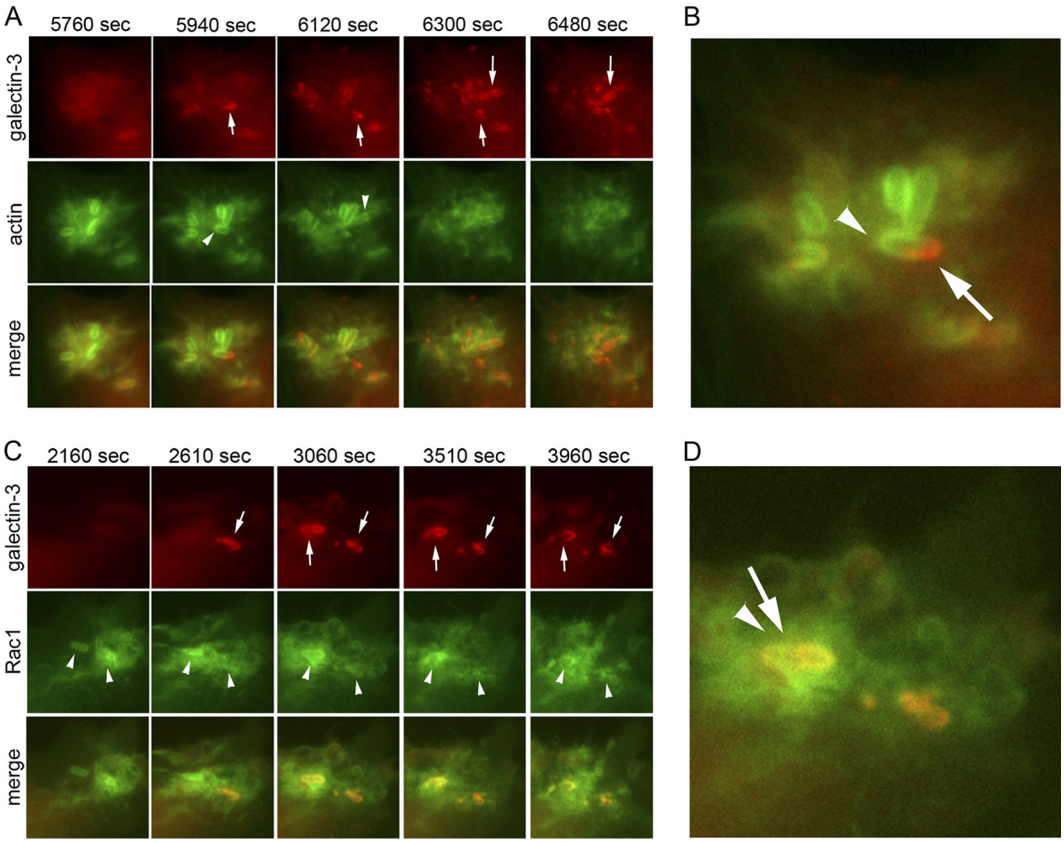

FIG 5 Hierarchies of host factor dispersal from the disassembling vacuoles. (A) HeLa cells were cotransfected with galectin 3-mOrange (arrow, red) and actin-EGFP (arrowhead, green) before being challenged with *S. flexneri*. Time lapse microscopy shows that actin disperses from the vacuole containing bacteria before its disassembly. Staining of the two factors is mutually exclusive. (B) Enlargement of an image from panel A. The arrowhead shows the actin signal (green) surrounding one moiety of a bacterium, and the arrow shows the other moiety with galectin 3 accumulation (red). (C) HeLa cells were cotransfected with galectin 3-mOrange (arrow, red) and Rac1-EGFP (arrowhead, green) before being challenged with *S. flexneri*. Rac1 surrounds the entering bacteria and remains associated with the galectin 3-positive membrane remnants after vacuolar rupture. (D) Enlargement of an image from panel C. The arrowhead and arrow point to the overlapping signal (orange) of Rac and galectin 3. Representative data from 7 independent experiments are shown.

3 (arrowheads) and actin (arrows) signals around the disassembling vacuoles were mutually exclusive. Furthermore, actin could not be readily identified around smaller vesicular structures potentially derived from disassembling vacuoles at later time points after the escape of *S. flexneri* to the cytoplasm. In contrast, the small GTPase Rac1 was also recruited to the vacuole containing bacteria; however, it remained located around the membrane remnants upon vacuolar rupture, colocalizing with galectin 3 (Fig. 5B and D; for more detail, see Movie S6 in the supplemental material). The tyrosine kinase Src (24) (see Fig. S1 in the supplemental material) is also recruited to the *Shigella*-containing vacuole, but this event was not seen with the kinase Abl and the small GTPase RhoA, which were both recruited rather diffusely or at the distal ends of the forming entry foci (Fig. 1). Together, these findings show that, despite simultaneous recruitment of the investigated host factors to the entering bacteria, the sequence of events during vacuolar disassembly appear to be temporally well organized.

IpgB1 accelerates the pace of invasion by *S. flexneri*. It has been reported that the *S. flexneri* T3SS effector IpgB1 mimics small GTPases to promote their entry into epithelial host cells (11, 12, 27). Using low multiplicities of infection (MOIs) (between 1 and 5) and following bacterial internalization at successive time points by gentamicin protection assay, we found that the *ipgB1* strain showed reduced entry. However, increasing the load of challenging bacteria or increasing the time periods of infection impeded the readout of this endpoint assay (data not shown). Therefore, we chose to track the dynamics of the time course of internalization and the recruitment of host factors to the bacterial entry site using the *ipgB1* mutant with the aim of measuring the effects on the entry kinetics. Performing time lapse microscopy on HeLa cells transfected with the host factors shown in Fig. 1 and 2, we found that the *ipgB1* mutant was able to enter host cells; however, the time periods of host factor recruitment to the bacterial contact site and entry were massively reduced (Fig. 6A and C; see Fig. S3 and Movie S7 in the supplemental material) compared to the wild-type bacteria (Fig. 6B and C; see Fig. S3 in the supplemental material). The wild-type phenotype was restored when the *ipgB1* complemented strain was used (see Fig. S3 in the supplemental material).

We also tested whether IpgB1 affected the subsequent step of vacuolar maturation and escape of the bacteria into the cytoplasm. To do this, we performed time lapse microscopy on HeLa cells coexpressing fluorescent actin and galectin 3, challenged with either the wild-type, *ipgB1*, or complemented strain (Fig. 7). Again, we found that the entry of the *ipgB1* strain was delayed (Fig. 7A;

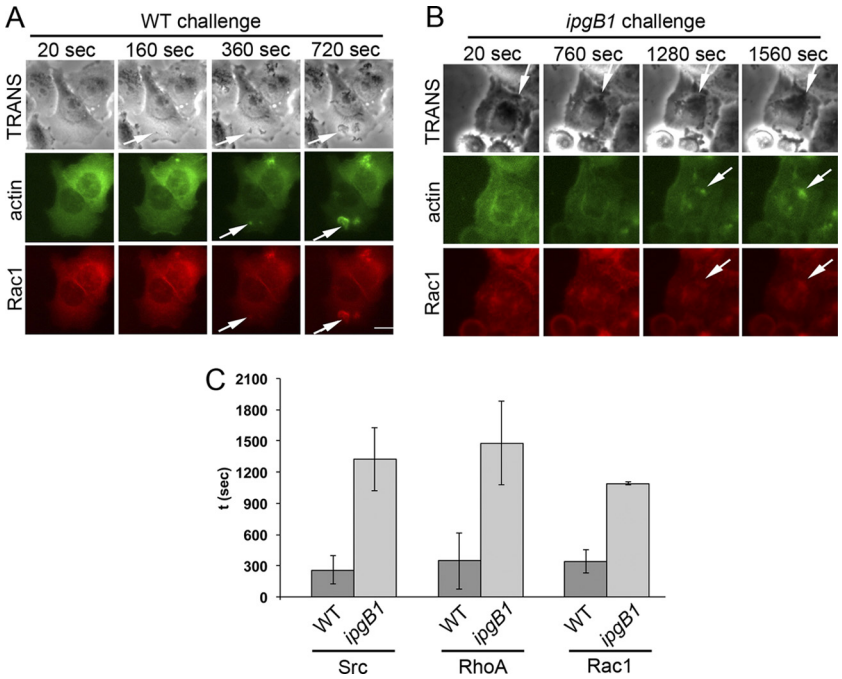

FIG 6 The *S. flexneri ipgB1* strain enters HeLa cells, but at a reduced rate. (A) Time lapse microscopy of cells cotransfected with actin and Rac1 and challenged with the *S. flexneri* wild-type strain. Arrows show bacterial entry sites. (B) Cells transfected similarly to those in panel A and challenged with an *S. flexneri ipgB1* mutant. Arrows show bacterial entry sites. (C) Quantification of the entry dynamics of the *S. flexneri* wild-type (WT) and *ipgB1* strains was performed using the time-lapse image series. Data from 5 independent experiments are shown. The error bars indicate SD.

see Movie S8 in the supplemental material). Interestingly, we identified some actin accumulation around the bacteria in contact with the host plasma membrane (Fig. 7A, middle; for more detail see Fig. S4 in the supplemental material), hinting at the involvement of multiple pathways for actin cytoskeletal rearrangement. Quantifying the time course of vacuolar escape, we were not able to measure significant differences between the *ipgB1*, the wild-type, and the complemented strains (Fig. 7B). In conclusion, the data presented in Fig. 6 and 7 suggest that IpgB1 represents a bacterial T3SS effector that accelerates the pace of *S. flexneri* entry into host cells as a means to boost bacterial infectivity but that it does not impact the subsequent steps.

DISCUSSION

Using time lapse microscopy, we demonstrated the simultaneous recruitment of host small GTPases and kinases to the site of *S. flexneri* entry into epithelial cells. Even though it is evident that bacterial invasion has to be highly organized, the functional hierarchies between the involved host factors have not been identified with precision (2, 7). So far, hierarchies of small GTPases have been described only in the case of *Salmonella* infection (28, 29).

Simultaneous host factor recruitment (Fig. 1 and 2) may call into question the importance of strict hierarchies during cellular invasion or may highlight the fact that the entry process is following not only one pathway, but multiple pathways, as previously proposed for *S. enterica* (13, 14). However, it also highlights the limitations of the performance of our microscopes with regard to both spatial and temporal resolution. Another fact that has to be considered is the activation of the signaling molecules involved; for example, GTPases can switch between GDP- and GTP-bound states, and kinases can be activated via phosphorylation. Such activities have already been taken into account by some studies on host-pathogen interactions, for example, in the case of *Yersinia*, using functionalized fluorescence resonance energy transfer (FRET) probes for the GTP state of small GTPases (39). Nevertheless, these studies require a high level of experimental sophistication, impeding its broad use throughout the scientific community. Considering the manifold and seemingly contradictory functions of the injected bacterial effectors on the host, such as actin polymerization via IpaC and its depolymerization via IpaA, we suggest that future studies will be required to reveal the precise recruitment of host factors and their dispersal (24). This will be facilitated once the precise enzymatic functions of the injected effectors have been revealed.

It is possible to track the step of vacuolar escape of *S. flexneri* with more precision. Recently, we have shown that this event takes place rapidly upon internalization (26, 34). Vacuolar escape has also been found for other cytoplasmic bacteria, for example, *Listeria* and *Rickettsia* (35). Strikingly, in this study, we show the rapid disassembly of the membrane remnants (Fig. 3) that have been reported to be coated with autophagy markers upon vacuolar rupture (8). This shows that the signaling events leading to the "digestion" of the membrane remnants have to be very rapid, efficient, and transient. PALM microscopy revealed the heterogeneous, patchy nature of the membrane remnants (Fig. 4). First, we found that the disassembled membranes were not hollow, highlighting their multilayered or micellar organization. Second, their resolvable size distribution spanned 30 to 300 nm (see Fig. S1 in the supplemental material). Based on these observations, we suggest that the membrane remnants are eventually disassembled or recycled, not only by a single mechanism, but by multiple mech-

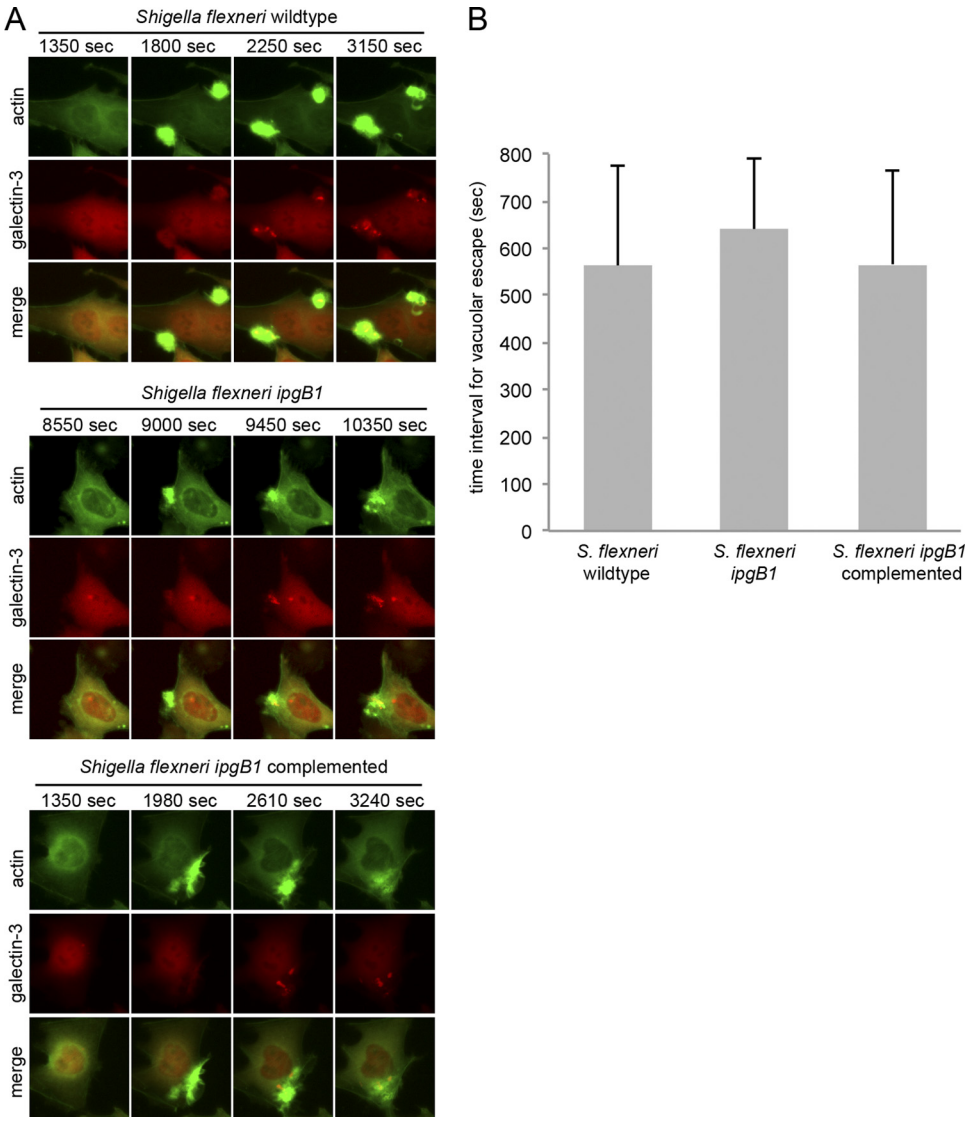

FIG 7 Effects of *Shigella* IpgB1 on entry and vacuolar disassembly. (A) Time lapse microscopy of HeLa cells cotransfected with actin-EGFP and galectin 3-mOrange challenged with the wild-type strain, with the *ipgB1*strain, or with the *ipgB1* strain complemented with IpgB1. The *ipgB1* mutant escaped efficiently from the endocytic vacuole. (B) Quantification of the time intervals between entry focus formation and escape of *S. flexneri* wild-type, *S. flexneri ipgB1*, and complemented strains from vacuoles. The wild-type bacteria escaped from the vacuoles at the same rate as the *ipgB1* mutant. Representative data from 4 independent experiments are shown. The error bars indicate SD.

anisms. Further, it is likely that the heterogeneous vesicular remnants result in the induction of multiple signaling pathways.

Taking advantage of our single-cell-based assays, we also found that some bacteria remained vacuole bound in vesicles coated with actin. It would be interesting to investigate the fate of these vacuole-bound bacteria, for example, if they are also targeted to the autophagy pathway. So far, it has been reported that cytoplasmic bacterial pathogens can be trapped within septin cages that send specific signals to trigger autophagy (22, 23). In addition to these signaling events, we suggest that future studies investigate whether septins can also be recruited to *S. flexneri* trapped within actin-coated vacuoles and whether the signals emanating from the trapped vacuolar bacteria are different from the signals emanating from cytoplasmic bacteria trapped in septin cages.

Where *S. flexneri* succeeded in escaping from the endocytic vacuoles, we noted that the dispersal of the host factors surrounding the cytoplasmic escaping bacteria appeared to be more organized than the recruitment during the initial steps of entry (Fig. 5). Since the membrane remnants appear to be targeted to the autophagy machinery, it will be important to investigate whether the sequential recruitment and dispersal of host factors around these remnants impacts the signaling cascades emanating from them.

Challenging host cells with a number of bacterial mutants, for example, with the translocon component IpaB or IpaC, results in very little or no invasion of the host cells (10). In contrast, mutant strains for other effectors show attenuated and subtle invasion phenotypes. One of these is the GEF IpgB1 that interferes with the ELMO/Dock180 pathway at the host plasma membrane upstream of the small GTPases (12, 27). An *S. flexneri* mutant strain for IpgB1 and IpgB2 was as invasive as the wild-type strain, indicating

that these homologous effectors have contradictory functions (11). In this work, we show that IpgB1 increases the pace of bacterial invasion, and we propose that the attenuated invasion phenotype of the *ipgB1* strain is caused by an alteration of the overall invasion time course (Fig. 6). This identified a bacterial T3SS effector as a pacemaker for infection targeting one precise step of the entry process. Strikingly, subsequent steps, such as the delay between entry and vacuolar escape, were not affected in the *ipgB1* mutant strain (Fig. 7). Often, loss-of-function studies of pathogen invasion, either using mutants or performing gene silencing via small interfering RNAs, result in phenotypes with a somewhat reduced but far from complete loss of infectivity (21). This can be a result of cellular plasticity or redundancy of host factor function. For example, this has been shown for *S. enterica*, which enters host cells via a pathway including the Arp2-Arp3 complex or via a myosin II-dependent pathway (13, 14). Nevertheless, pathway plasticity/redundancy is only one explanation of attenuated phenotypes. Consequently, we suggest that future studies should focus on the implication of merely kinetic effects of invasion, and we propose that time lapse investigations are perfectly suited for such studies. We are convinced that such kinetic studies will shift our idea of the functions of numerous bacterial effectors and involved host factors during the dynamic interplay between pathogens and their hosts.

Our results indicate the rapidity of events around the entering pathogens and also highlight the fact that perturbation of the system results in altered time courses of the invasion process. Microscopy-based high-throughput screens have become widely popular to investigate host-pathogen interactions in single cells (33). For the most part, they are performed as endpoint assays yielding only a single time point of the investigated events. Screens performed by different research groups investigating the same phenomenon have yielded different, even opposing, results (33). One possible explanation lies in the limitations of the assays used for the studies. Having described galectin 3 as a marker for vacuolar rupture, our work underlines the fact that it is particularly suited for time lapse investigation (30). On the other hand, the rapid disassembly of the membrane remnants upon rupture hampers efficient signal detection at later time points of infection (Fig. 3). Therefore, care must be taken in choosing the appropriate time points when using galectin 3 in endpoint assays in fixed samples.

ACKNOWLEDGMENTS

We thank C. Parsot, R. Tsien, J. Swanson, and A. M. Pendergast for providing us with plasmids and/or bacterial strains. We are particularly thankful to M. Lelek for support in the PALM experiments. We acknowledge the members of the PFID at the Institut Pasteur for excellent microscopy support.

S.E. was supported by a grant from the Fondation Schlumberger pour l'Education et la Recherche. J.C.S. and C.D.R. were the recipients of fellowships from the Portuguese Fundação para a Ciência e Tecnologia, FCT (SFRH/BD/51006/2010 and SFRH/BPD/41004/2007, respectively). C.D.R. is presently a Marie Curie fellow.

REFERENCES

1. **Betzig E, et al.** 2006. Imaging intracellular fluorescent proteins at nanometer resolution. Science **313**:1642–1645.
2. **Bobard A, Mellouk N, Enninga J.** 2011. Spotting the right location—imaging approaches to resolve the intracellular localization of invasive pathogens. Biochim. Biophys. Acta **1810**:297–307.
3. **Bougneres L. Girardin SE, et al.** 2004. Cortactin and Crk cooperate to trigger actin polymerization during Shigella invasion of epithelial cells. J. Cell Biol. **166**:225–235.
4. **Bourdet-Sicard R, et al.** 1999. Binding of the Shigella protein IpaA to vinculin induces F-actin depolymerization. EMBO J. **18**:5853–5862.
5. **Burton EA, Plattner R, Pendergast AM.** 2003. Abl tyrosine kinases are required for infection by Shigella flexneri. EMBO J. **22**:5471–5479.
6. **Clerc P, Sansonetti PJ.** 1987. Entry of Shigella flexneri into HeLa cells: evidence for directed phagocytosis involving actin polymerization and myosin accumulation. Infect. Immun. **55**:2681–2688.
7. **Dunn JD, Valdivia RH.** 2010. Uncivil engineers: Chlamydia, Salmonella and Shigella alter cytoskeleton architecture to invade epithelial cells. Future Microbiol. **5**:1219–1232.
8. **Dupont N, et al.** 2009. Shigella phagocytic vacuolar membrane remnants participate in the cellular response to pathogen invasion and are regulated by autophagy. Cell Host Microbe **6**:137–149.
9. **Ehsani S, Rodrigues CD, Enninga J.** 2009. Turning on the spotlight—using light to monitor and characterize bacterial effector secretion and translocation. Curr. Opin. Microbiol. **12**:24–30.
10. **Enninga J, Mounier J, Sansonetti P, Tran Van Nhieu G.** 2005. Secretion of type III effectors into host cells in real time. Nat. Methods **2**:959–965.
11. **Hachani A, et al.** 2008. IpgB1 and IpgB2, two homologous effectors secreted via the Mxi-Spa type III secretion apparatus, cooperate to mediate polarized cell invasion and inflammatory potential of Shigella flexenri. Microbes Infect. **10**:260–268.
12. **Handa Y, et al.** 2007. Shigella IpgB1 promotes bacterial entry through the ELMO-Dock180 machinery. Nat. Cell Biol. **9**:121–128.
13. **Hanisch J, et al.** 2010. Molecular dissection of Salmonella-induced membrane ruffling versus invasion. Cell Microbiol. **12**:84–98.
14. **Hanisch J, et al.** 2011. Activation of a RhoA/myosin II-dependent but Arp2/3 complex-independent pathway facilitates Salmonella invasion. Cell Host Microbe **9**:273–285.
15. **Henriques R, et al.** 2010. QuickPALM: 3D real-time photoactivation nanoscopy image processing in ImageJ. Nat. Methods **7**:339–340.
16. **Hess ST, Girirajan TP, Mason MD.** 2006. Ultra-high resolution imaging by fluorescence photoactivation localization microscopy. Biophys. J. **91**:4258–4272.
17. **Hoppe AD, Swanson JA.** 2004. Cdc42, Rac1, and Rac2 display distinct patterns of activation during phagocytosis. Mol. Biol. Cell **15**:3509–3519.
18. **Huang Z, et al.** 2009. Structural insights into host GTPase isoform selection by a family of bacterial GEF mimics. Nat. Struct. Mol. Biol. **16**:853–860.
19. **Konradt C, et al.** 2011. The Shigella flexneri type three secretion system effector IpgD inhibits T cell migration by manipulating host phosphoinositide metabolism. Cell Host Microbe **9**:263–272.
20. **Kotloff KL, et al.** 1999. Global burden of Shigella infections: implications for vaccine development and implementation of control strategies. Bull. World Health Organ. **77**:651–666.
21. **Misselwitz B, et al.** 2011. RNAi screen of Salmonella invasion shows role of COPI in membrane targeting of cholesterol and Cdc42. Mol. Syst. Biol. **7**:474.
22. **Mostowy S, et al.** 2010. Entrapment of intracytosolic bacteria by septin cage-like structures. Cell Host Microbe **8**:433–444.
23. **Mostowy S, et al.** 2011. p62 and NDP52 proteins target intracytosolic Shigella and Listeria to different autophagy pathways. J. Biol. Chem. **286**:26987–26995.
24. **Mounier J, et al.** 2009. The IpaC carboxyterminal effector domain mediates Src-dependent actin polymerization during Shigella invasion of epithelial cells. PLoS Pathog. **5**:e1000271. doi:10.1371/journal.ppat.1000271.
25. **Nhieu GT, Enninga J, Sansonetti P, Grompone G.** 2005. Tyrosine kinase signaling and type III effectors orchestrating Shigella invasion. Curr. Opin. Microbiol. **8**:16–20.
26. **Nothelfer K, Dias Rodrigues C, Bobard A, Phalipon A, Enninga J.** 2011. Monitoring Shigella flexneri vacuolar escape by flow cytometry. Virulence **2**:54–57.
27. **Ohya K, Handa Y, Ogawa M, Suzuki M, Sasakawa C.** 2005. IpgB1 is a novel Shigella effector protein involved in bacterial invasion of host cells. Its activity to promote membrane ruffling via Rac1 and Cdc42 activation. J. Biol. Chem. **280**:24022–24034.
28. **Patel JC, Galan JE.** 2006. Differential activation and function of Rho GTPases during Salmonella-host cell interactions. J. Cell Biol. **175**:453–463.
29. **Patel JC, Galan JE.** 2008. Investigating the function of Rho family GTPases during Salmonella/host cell interactions. Methods Enzymol. **439**:145–158.

30. **Paz I, et al.** 2010. Galectin-3, a marker for vacuole lysis by invasive pathogens. Cell Microbiol. **12**:530–544.
31. **Perrett CA, Jepson MA.** 2007. Applications of cell imaging in Salmonella research. Methods Mol. Biol. **394**:235–273.
32. **Pizarro-Cerda J, Cossart P.** 2006. Bacterial adhesion and entry into host cells. Cell **124**:715–727.
33. **Prudencio M, Lehmann MJ.** 2009. Illuminating the host—how RNAi screens shed light on host-pathogen interactions. Biotechnol. J. **4**:826–837.
34. **Ray K, et al.** 2010. Tracking the dynamic interplay between bacterial and host factors during pathogen-induced vacuole rupture in real time. Cell Microbiol. **12**:545–556.
35. **Ray K, Marteyn B, Sansonetti PJ, Tang CM.** 2009. Life on the inside: the intracellular lifestyle of cytosolic bacteria. Nat. Rev. Microbiol. **7**:333–340.
36. **Sansonetti PJ, Ryter A, Clerc P, Maurelli AT, Mounier J.** 1986. Multiplication of Shigella flexneri within HeLa cells: lysis of the phagocytic vacuole and plasmid-mediated contact hemolysis. Infect. Immun. **51**: 461–469.
37. **Schroeder GN, Hilbi H.** 2008. Molecular pathogenesis of Shigella spp.: controlling host cell signaling, invasion, and death by type III secretion. Clin. Microbiol. Rev. **21**:134–156.
38. **Terry CM, et al.** 2008. The C-terminus of IpaC is required for effector activities related to Shigella invasion of host cells. Microb. Pathog. **45**:282–289.
39. **Wong KW, Mohammadi S, Isberg RR.** 2006. Disruption of RhoGDI and RhoA regulation by a Rac1 specificity switch mutant. J. Biol. Chem. **281**: 40379–40388.